Finite-size and finite bond dimension effects of tensor network renormalization

Atsushi Ueda [1,*] and Masaki Oshikawa [1,2,3]

[1]*Institute for Solid State Physics, University of Tokyo, Kashiwa 277-8581, Japan*
[2]*Kavli Institute for the Physics and Mathematics of the Universe (WPI), The University of Tokyo, Kashiwa, Chiba 277-8583, Japan*
[3]*Trans-scale Quantum Science Institute, University of Tokyo, Bunkyo-ku, Tokyo 113-0033, Japan*

We propose a general procedure for extracting the running coupling constants of the underlying field theory of a given classical statistical model on a two-dimensional lattice, combining tensor network renormalization (TNR) and the finite-size scaling theory of conformal field theory. By tracking the coupling constants at each scale, we are able to visualize the renormalization group flow and demonstrate it with the classical Ising and three-state Potts models. Furthermore, utilizing this methodology, we reveal the limitations due to finite bond dimension D on TNR applied to critical systems. We find that a finite correlation length is imposed by the finite bond dimension in TNR, and it can be attributed to an emergent relevant perturbation that respects the symmetries of the system. The correlation length shows the same power-law dependence on D as the "finite entanglement scaling" of the matrix product states.

I. INTRODUCTION

The universality of critical phenomena is one of the most intriguing and important concepts in statistical physics. The renormalization group (RG), proposed by Wilson [1–3], provides a conceptual framework to comprehend and characterize this universality.

In the RG framework, a universality class of critical phenomena is governed by an RG fixed point in the "theory space." Theory space is the abstract space of all possible models or theories that can describe a physical system. Each point in this space represents a unique combination of the parameters of the theory or, more concretely, the corresponding Hamiltonian or action. In the context of the RG, we explore this "theory space" by starting from a specific point in the theory space and applying the RG transformations. These transformations effectively move us through the theory space, changing the values of the parameters as we coarse grain the system. Importantly, models within the same universality class converge to an identical position through the RG transformations. This allows for diverse critical phenomena to be comprehended in terms of perturbations to the fixed-point Hamiltonian and their respective scaling behavior.

This theoretical approach has directly facilitated the development of concrete schemes for the calculation of critical exponents. A prime example is the ϵ expansion for the ϕ^4 theory in $4 - \epsilon$ dimensions [4,5]. While the practical utility of such a scheme for calculating critical exponents may appear to be limited, it is imperative to underscore that the RG framework establishes the conceptual foundation for understanding the universality of critical phenomena.

In particular, the fixed point displays conformal invariance in two dimensions, thereby simplifying the associated theory which is described by a conformal field theory (CFT). The effective Hamiltonian near the RG fixed-point Hamiltonian, denoted $\hat{H}_{\text{CFT}}$, can be expressed as follows:

$$\hat{H} = \hat{H}_{\text{CFT}} + \sum_j g_j \int_0^L dx\, \hat{\Phi}_j(x). \tag{1}$$

In this expression, $\hat{\Phi}_j(x)$ represents a scaling operator with a scaling dimension x_j, and g_j denotes the corresponding coupling constant. In two dimensions, the running coupling constants g_j are renormalized as $g_j \propto L^{2-x_j}$ as functions of a scale $l = \ln(L/a)$. In general, there are only a few *RG-relevant* coupling constants with $x_j < 2$, which increase as the scale l increases.

There also exists *RG-irrelevant* coupling constants with $x_j > 2$ that decrease as the scale l increases. Despite their occasional significance, the principal characteristics of critical phenomena can be outlined primarily by considering the limited number of RG-relevant coupling constants. Differential equations, termed RG equations, frequently describe the evolution of these running coupling constants as functions of the scale l. Field theory methods frequently serve as the basis for deriving these RG equations.

However, it is worth noting that the exact determination of RG equations may not always be feasible when the corresponding field theory is not solvable. Moreover, the application of RG to lattice models has generally been challenging for quantitative calculations. While offering an intuitive understanding of RG, the "block-spin transformation" method falls short as a practical computational method for lattice models. Overall, early RG schemes for lattice models saw limited success, the notable exception being Wilson's numerical renormalization group for impurity problem [3].

*aueda@issp.u-tokyo.ac.jp

Subsequently, density matrix renormalization group (DMRG) [6] emerged as a highly effective numerical algorithm for one-dimensional quantum many-body systems. Despite its name, DMRG is typically employed as a numerical algorithm with less emphasis on RG flows in the "theory space."

More recently, the development of tensor network renormalization (TNR) [7–12] opened a way to implement numerical schemes for a wide range of lattice models in a manner more faithful to the original concept of RG. Notably, it is possible to obtain a fixed-point tensor after multiple iterations of TNR steps. This fixed-point tensor encapsulates critical information about the infrared (IR) fixed point, including conformal data.

Regarding RG flow, there have been numerous previous studies [8,10,11,13,14]. Yet, a generic and quantitative framework for calculating RG flows remains elusive, primarily due to challenges in maintaining the correlation between the changes in numerically obtained tensor networks and the RG flow within the theory space.

In this paper, we first propose an efficient and quantitative scheme to extract the RG flow numerically from TNR, discussed in Sec. III. This involves comparing the finite-size spectrum of the transfer matrix with CFT. Concrete examples, such as the numerical results of the Ising and three-state Potts models, are employed to validate the theoretical predictions. Our method also provides an efficient and accurate estimation of the critical point, extending the "level spectroscopy" technique previously developed for Berezinskii-Kosterlitz-Thouless (BKT) transitions [15,16].

Leveraging this methodology, we uncover the effects of finite bond dimension D on TNR at criticality in Sec. IV. The finite-bond approximation of tensors constrains the effective correlation length, preventing the attainment of a "true fixed-point tensor" corresponding to a nontrivial RG fixed point through repeated TNR procedures. While this phenomenon was reported in earlier studies [7–12], it has been often overlooked. Our numerical results suggest that the finite bond dimension effects can be attributed to an emergent relevant perturbation that respects the symmetry of the lattice model. Furthermore, we demonstrate that the finite correlation length that is imposed by the finite bond dimension scales in the same way as in matrix product states (MPS).

We note that some of the methods and observations discussed in this paper were previously reported in our earlier publication [16], where they were applied to the classical XY model. The goal of this paper is to illustrate the more widespread applicability of this approach and deliver a more comprehensive analysis of the finite bond dimension effects.

Sample codes necessary to reproduce the figures presented in this paper, along with introductory reviews on TRG and TNR, are accessible via Jupyter notebooks at the GitHub repository [17].

II. REVIEW ON TENSOR NETWORK RENORMALIZATION AND CONFORMAL FIELD THEORY

A. Tensor network renormalization

The tensor network is a numerical technique used to represent the partition function of statistical models. The partition
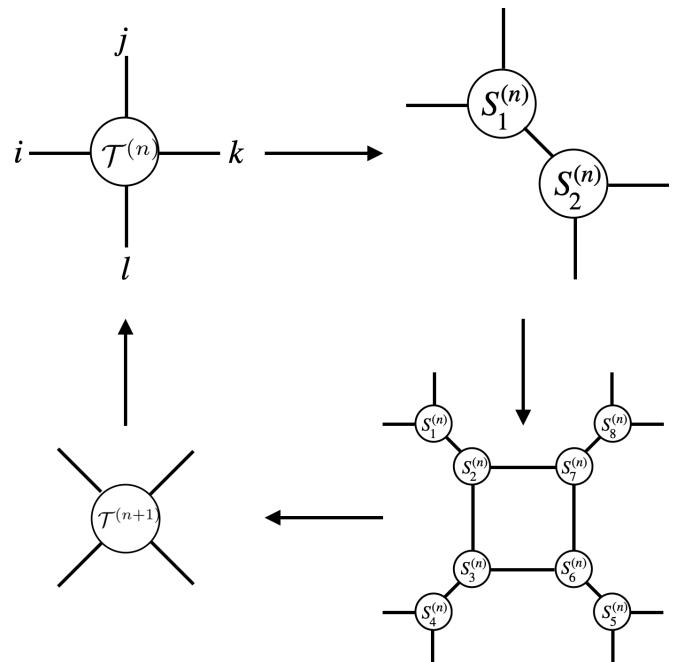

FIG. 1. A schematic picture of the tensor network renormalization. The effective local Boltzmann weight at nth RG step $\mathcal{T}^{(n)}$ is decomposed into the two three-leg tensors and recombined as $\mathcal{T}^{(n+1)}$. The effective system size enlarges by $\sqrt{2}$ each RG step. The typical bond dimension and the maximum number of RG steps employed in this paper are $D \leqslant 40$, and RG steps $\leqslant 30$, respectively.

functions of two-dimensional statistical models with a system size of L can be expressed through the contraction of L^2 tensors. Each tensor represents a local Boltzmann weight, and its dimensions correspond to physical degrees of freedom. For instance, the local tensor of the Ising model on the square lattice is a four-leg tensor $\mathcal{T}_{ijkl}^{(1)} = e^{\beta(s_i s_j + s_j s_k + s_k s_l + s_l s_i)}$. The tensor network representation often provides an efficient method for simulating complex systems.

However, the exact contraction of L^2 tensors is generally impracticable for larger system sizes due to the constraints imposed by the high-dimensional Hilbert space. TNR aims to circumvent this issue by utilizing the principles of renormalization group theory. During each step of the RG process, $\mathcal{T}^{(n)}$ is coarse grained to $\mathcal{T}^{(n+1)}$ via a series of decompositions and recombinations, as illustrated in Fig. 1. Starting from the local tensor $\mathcal{T}^{(1)}$, we can simulate a system size of $L = \sqrt{2}^n$ after n RG steps. The process of coarse graining in TNR involves numerical truncation, reducing the number of degrees of freedom while preserving essential physics. Consequently, TNR facilitates efficient numerical simulation of complex systems.

B. Critical phenomena under conformal invariance

The following sections mainly discuss the Ising and three-state Potts models on the square lattice. The energies (classical Hamiltonian) of the Ising and three-state Potts models are

$$\mathcal{E}_{\text{Ising}} = -\sum_{\langle i,j \rangle} s_i s_j - h \sum_i s_i, \qquad (2)$$

$$\mathcal{E}_{\text{Potts}} = -\sum_{\langle i,j \rangle} \delta_{s_i,s_j}, \qquad (3)$$

where $s_i = \pm 1$ (Ising) and $s_i = 0, 1, 2$ (three-state Potts). The first terms and h represent the nearest-neighbor interactions and the magnetic field. Employing the temperature T, the Boltzmann weight is defined as $e^{-\mathcal{E}/T}$, where we set the Boltzmann constant to unity. Our primary focus in the main text is the Ising model, while a detailed discussion of the three-state Potts model is provided in the Appendix. The Ising model reaches its critical point at $(T, h) = (T_c, 0)$, where $T_c = 2/\ln(1 + \sqrt{2})$. At this criticality, physical quantities like the spin-spin correlation function are governed by the Ising CFT, which comprises three primary operators: the identity operator I, magnetic operator σ, and energy operator ϵ.

In the context of the lattice model, a shift from the critical temperature and the application of a magnetic field correspond to the perturbative insertion of ϵ and σ into the effective Hamiltonian. As a result, σ is odd in the $\mathbb{Z}_2$ spin flip, while I and ϵ are even. Given the operator structure of the CFT, certain quantities are consequently fixed.

The two-point correlation function is defined as

$$\langle \Phi_i(r_i) \Phi_j(r_j) \rangle = \frac{\delta_{i,j}}{|r_i - r_j|^{2x_i}},$$

where Φ_i represents a primary operator, and $x_I = 0$, $x_\sigma = \frac{1}{8}$, and $x_\epsilon = 1$ are the scaling dimensions. In a similar vein, the three-point correlation function adopts a universal form, represented as

$$\langle \Phi_i(r_i) \Phi_j(r_j) \Phi_k(r_k) \rangle = \frac{C_{ijk}}{|r_i - r_j|^{\Delta_{ij}^k} |r_j - r_k|^{\Delta_{jk}^i} |r_k - r_i|^{\Delta_{ki}^j}},$$

where C_{ijk} is an operator product expansion (OPE) coefficient, and $\Delta_{ij}^k = x_i + x_j - x_k$. The nonzero OPE coefficients are given as follows:

$$C_{III} = C_{I\sigma\sigma} = C_{I\epsilon\epsilon} = 1, \tag{4}$$

$$C_{\sigma\sigma\epsilon} = \tfrac{1}{2}. \tag{5}$$

The permutation of the indices does not change the OPE coefficients.[1] (For further details of CFT, we suggest readers see Ref. [18].) The collection of information on the scaling dimension x_i and C_{ijk}, referred to as the CFT data, is crucial to understanding critical phenomena. As such, determining the CFT from a numerical standpoint is of paramount importance.

III. COMPUTATION OF FIELD-THEORY DATA AND RG FLOW FROM TNR

A. Scaling dimensions

For simplicity, let us consider a classical statistical model on the square lattice with nearest-neighbor interactions only. Then the local Boltzmann weight can be represented by a tensor $\mathcal{T}$ with four open indices, and the partition function is given by contraction of a tensor network which consists of the tensor $\mathcal{T}$.

More specifically, the partition function $Z(L_x, L_y)$ for the system of the size $L_x \times L_y$ is given by the contraction of the network of $L_x \times L_y$ identical tensors $\mathcal{T}$.

Under a single step of TNR, the length scale represented by a single tensor is renormalized by $\sqrt{2}$. After N steps, the renormalized tensor becomes $\mathcal{T}(L)$, which represents the length scale $L = \sqrt{2}^N$. As $\mathcal{T}(L)$ is equivalent to the $L \times L$ contracted tensor network up to truncation errors, contractions of the horizontal and vertical legs yield the partition function $Z(L, L)$ in periodic boundary condition (PBC). Similarly, contracting only the legs in the x direction gives the L stacks of the transfer matrix in y-direction. Since one can regard the transfer matrix as the imaginary-time evolution operator of corresponding one-dimensional quantum systems, its eigenvalues $\lambda_n(L)$ are related to the energy levels $E_n(L)$ of the quantum system as $\lambda_n(L) = \exp[-LE_n(L)]$. For convenience, we define the rescaled energy levels $x_n(L)$ by $E_n(L) - E_0(L) = 2\pi x_n(L)/L^2$ to obtain

$$\frac{\lambda_n(L)}{\lambda_0(L)} = \exp[-2\pi x_n(L)]. \tag{6}$$

Exactly at the criticality, this rescaled energy level $x_n(L)$ coincides with the scaling dimension x_n in the thermodynamic limit ($L \to \infty$) [19–21].

If the system is off-critical and without a spontaneous symmetry breaking, the rescaled energy level of the "first excitation" is asymptotically proportional to the system size as $\Delta L/(2\pi)$, where Δ is the inverse correlation length (excitation gap) in the thermodynamic limit.

Summarizing these observations, naively speaking, we can judge whether the system is critical or not by looking at the asymptotic behavior of the rescaled energy levels $x_n(L)$. If they grow linearly in L, the system is off-critical. If they approach to constants, the system is critical, and the scaling dimensions of the operators can be read off from the asymptotic values of $x_n(L)$ in the thermodynamic limit. While this can be a useful guide, there are corrections from RG-irrelevant perturbations and, more importantly, due to the limitation of a finite bond dimension, as we will discuss later.

B. Operator product expansion coefficients

Operator product expansion is another fundamental concept in field theory and statistical mechanics [22,23]. Since OPE coefficients determine the structure of the field theory, their computation is quite important. Numerical computation of OPE coefficients [24,25] has not been so straightforward compared to that of scaling dimensions. Here, we present a simpler way to compute them, which is applicable to TRG [7], HOTRG [26], and Loop-TNR [10].
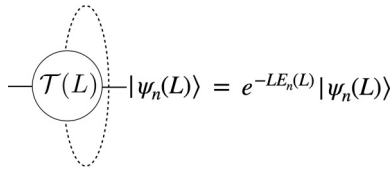
As explained in the previous section, the renormalized tensor $\mathcal{T}^{(N)}$ contracted in the x direction is a transfer matrix in the y direction. While the eigenvalues of the transfer matrix correspond to the energy or scaling dimension of the primary operators, the eigenvectors thereof are the wave functions of the corresponding "primary states" $|\psi_n(L)\rangle$. This is

---

[1]The combination of the indices in nonzero C_{ijk} preserves $\mathbb{Z}_2$ symmetry.

[2]In the classical systems, the characteristic velocity v, playing the role of the speed of light, is unity because the system invariant under the exchange of the x and y axes.

TABLE I. The numerically obtained OPE coefficients of the Ising CFT from TRG. The bond dimension and the system size are $D = 56$ and $L = 16\sqrt{2}$(9 RG steps), respectively.

ψ_α	ψ_β, ψ_γ	$C_{\alpha\beta\gamma}$	$2^{2\Delta_\beta + 2\Delta_\gamma - \Delta_\alpha} A_{\alpha\beta\gamma} / A_{III}$
I	σ, σ	1	0.8938
σ	σ, I	1	0.9473
I	ϵ, ϵ	1	0.9966
ϵ	ϵ, I	1	0.9968
ϵ	σ, σ	0.5	0.5007
σ	σ, ϵ	0.5	0.2705

graphically represented below.

$$-\boxed{\mathcal{T}(L)}-|\psi_n(L)\rangle \ = \ e^{-LE_n(L)}|\psi_n(L)\rangle$$

Note that the tensor has been rotated for ease of viewing. We do not change the contracted index. Likewise, we can compute the wave functions of the system size $2L$ as depicted below.

$$\begin{matrix}-\boxed{\mathcal{T}(L)}-\\-\boxed{\mathcal{T}(L)}-\end{matrix}\ |\psi_n(2L)\rangle = e^{-LE_n(2L)}|\psi_n(2L)\rangle$$
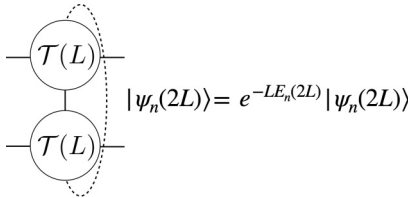
$|\psi_n(L)\rangle$ and $|\psi_n(2L)\rangle$ are one-leg and two-leg tensors, respectively. Thus, one can calculate the overlaps $|\psi_\alpha(2L)\rangle$ and $|\psi_\beta(L)\rangle \otimes |\psi_\gamma(L)\rangle$ by contracting the indices.

In CFT, the overlap $\langle\psi_\alpha(2L)|\psi_\beta(L)\psi_\gamma(L)\rangle$ is proportional to the "pants diagram" of path integrals [27–29], and the OPE coefficient and the overlap are related as

$$\frac{A_{\alpha\beta\gamma}}{A_{III}} = 2^{\Delta_\alpha - 2\Delta_\beta - 2\Delta_\gamma} C_{\alpha\beta\gamma}, \tag{7}$$

where $A_{\alpha\beta\gamma}$, Δ, and I are $\langle\psi_\alpha(2L)|\psi_\beta(L)\psi_\gamma(L)\rangle$, the scaling dimension, and the identity operator, respectively. In most cases, the identity operator corresponds to the ground state. We benchmark our method by the critical Ising model. Table I shows the numerically obtained OPE coefficients by TRG [7] at $L = 16\sqrt{2}$ and $D = 56$. Naturally, there are finite-size corrections to Eq. (7). Since Eq. (7) is exact in the thermodynamic limit, using a very large system size L might appear desirable. However, as we will discuss later in Sec. IV, corrections due to the finite bond dimension effect appear for system sizes larger than a correlation length $\xi(D)$.[3] As reported in Ref. [29], the finite-size effects are significant for $C_{\sigma\sigma\epsilon}$ and $C_{\epsilon\epsilon I}$. Nevertheless, even with the moderate size $L = 16\sqrt{2}$, the obtained values $C_{I\epsilon\epsilon} = 0.9966$ and $C_{\epsilon\sigma\sigma} = 0.5007$ are rather close to exact CFT results. While we tested our method by the simplest algorithm, Levin and Nave's TRG, the method for calculating

---

[3]This effect is even stronger and nontrivial for TRG.

OPE is straightforwardly applicable to other TRG and TNR algorithms, such as HOTRG [26].

C. Level spectroscopy

As we have mentioned earlier, the rescaled energy levels $x_n(L)$ in Eq. (6) would be independent of the scale L and give the scaling dimensions of the corresponding operators, if the system were exactly described by a CFT. However, the rescaled energy levels of a lattice model generally depend on the system size L, as the effective Hamiltonian of the system contains perturbations to the CFT as in Eq. (1).

The rescaled energy levels in a finite-size perturbed CFT are given as [19,20]

$$x_n(L) = x_n + 2\pi \sum_j C_{nnj} g_j(L), \tag{8}$$

where $g_j(L)$ scales as $\propto L^{2-x_j}$. Comparing Eq. (6) from TNR and Eq. (8) from the conformal perturbation theory, we can obtain the running coupling constants $g_j(L)$ at each scale from the finite-size effect $\delta x_n(L) = x_n(L) - x_n$.

An immediate application of this observation is an accurate determination of the critical point. While such a framework is dubbed "level spectroscopy" was developed for BKT transition, which is notoriously difficult for standard finite-size scaling analysis, first for quantum spin systems in one dimension [15] and recently extended for classical statistical systems in two dimensions using TNR [16], the basic idea is also applicable to more conventional critical phenomena such as in the Ising model.

The RG fixed point for the two-dimensional Ising model has two relevant operators, the energy density ϵ and the magnetization density σ. The coupling constant g_ϵ for ϵ is proportional to the deviation of the temperature from the critical point, and also scaled $\sim L$ in the small coupling limit $g_\epsilon \ll 1$ because $x_\epsilon = 1$. Thus,

$$g_\epsilon(L) \sim \alpha(T - T_c)L, \tag{9}$$

when $g_\epsilon(L) \ll 1$. Likewise, the coupling g_σ is proportional to the magnetic field h and scaled $\sim L^{15/8}$ because $x_\sigma = \frac{1}{8}$.

Although the Ising critical phenomena are mostly described by the two relevant coupling constants g_ϵ and g_σ, more accurate description can be obtained by including irrelevant perturbations. Including the leading irrelevant operators, namely, the irrelevant operators with the smallest scaling dimension permitted by the symmetries, we obtain

$$H = H_{\text{Ising}}^* + \int_0^L dx[g_\sigma \sigma(x) + g_\epsilon \epsilon(x) \\ + g_{T^2} T_{\text{cyl}}^2(x) + g_{\bar{T}^2} \bar{T}_{\text{cyl}}^2(x)], \tag{10}$$

where T_{cyl} and $\bar{T}_{\text{cyl}}$ are the holomorphic and antiholomorphic parts of stress tensor on a cylinder [20]. The holomorphic part T_{cyl} of the stress tensor on a cylinder is related to that on the infinite plane $T_{zz}(z)$ via the conformal mapping $z = e^{2\pi w/L}$, where $w = \tau + ix$ and $0 \leqslant x < L$. More explicitly, $T_{zz}(z)$ transforms as

$$T_{\text{cyl}}(w) = \left(\frac{2\pi}{L}\right)^2 \left(z^2 T_{zz}(z) - \frac{c}{24}\right). \tag{11}$$

TABLE II. The finite-size scaling dimension of the Ising model. α is a constant determined from the second-order perturbation. Since g_{T^2} and $g_{\bar{T}^2}$ decay in the same manner, we write them as g.

Model	Operator	Rescaled energy level
Ising model	$x_\sigma(L)$	$\frac{1}{8} + \alpha_\sigma^\sigma g_\sigma^2 + \pi g_\epsilon + \alpha_\sigma^\epsilon g_\epsilon^2 - \frac{7}{768}\pi g$
	$x_\epsilon(L)$	$1 + \alpha_\epsilon^\sigma g_\sigma^2 + \alpha_\epsilon^\epsilon g_\epsilon^2 + \frac{7}{48}\pi g$

This leads to

$$T_{\text{cyl}}(x) = \frac{2\pi}{L}\left(\sum_{n=-\infty}^{\infty} L_n e^{2\pi i x/L} - \frac{c}{24}\right), \quad (12)$$

where c is the central charge characterizing the CFT, and L_n's are generators of the Virasoro algebra defined by

$$T_{zz}(z) = \sum_{n=-\infty}^{\infty} \frac{L_n}{z^{n+2}}, \quad (13)$$

in terms of the holomorphic part T_{zz} of the energy-momentum tensor on the infinite plane. Inserting the above T_{cyl} and integrating over $0 \leqslant x < L$ with an appropriate regularization, the g_{T^2} term of the perturbation is given as [30]

$$\int dx\, T_{\text{cyl}}^2(x) = L_0^2 - \frac{c+2}{12}L_0 + 2\sum_{n=1}^{\infty} L_{-n}L_n + \frac{c(22+5c)}{2880}.$$

Only the first and second terms affect the energy levels, and the contributions to $x_\sigma(L)$ and $x_\epsilon(L)$ are calculated to be $-\frac{7}{768}g_{T^2}$ and $\frac{7}{48}g_{T^2}$, respectively. The computation of the contributions from $\bar{T}^2$ is exactly the same, and we denote their sum as g. These operators are the leading irrelevant operators for the Ising model on the square lattice. Although they break the continuous rotation symmetry (which corresponds to the Lorentz invariance in the Minkowski space-time), they are allowed on the square lattice, which is invariant only under the discrete C_4 rotation. The calculation of $x_\sigma(L)$ and $x_\epsilon(L)$ is straightforward, and they are shown in Table II.[4]

While the exact critical point is known for the Ising model on the square lattice, let us demonstrate the determination of the critical point from the TNR spectrum without using prior knowledge of the critical point (but utilizing the CFT data, assuming that we identify the universality class). Since we are interested in the critical point at zero magnetic fields, we can set $g_\sigma \propto h = 0$. The simplest way to determine the critical point is to look at the lowest rescaled energy level $x_\sigma(L)$ in the lowest order of the relevant coupling constant g_ϵ, ignoring the irrelevant perturbation g. Within this approximation, the shift $\delta x_\sigma(L) = x_\sigma(L) - x_\sigma$ vanishes at the critical point $T = T_c$ where $g_\epsilon = 0$. Away from the critical point, $\delta x_\sigma(L)$ is nonzero and grows proportionally to L because $g_\epsilon(L)$ scales as L. Because of this, we can identify the critical point with the temperature where $\delta x_\sigma(L) = 0$ is observed in the TNR spectrum. However, this estimate suffers from the corrections due to the leading irrelevant perturbations T_{cyl}^2 and $\bar{T}_{\text{cyl}}^2$. Since
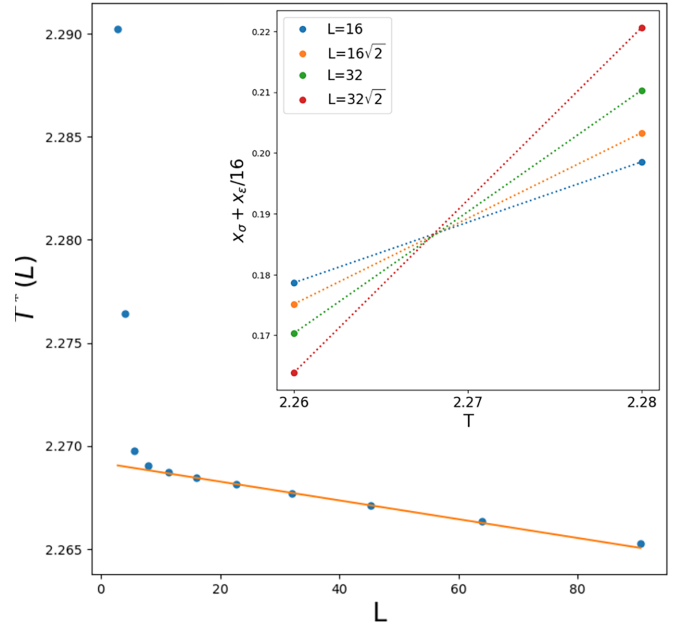
FIG. 2. Example of estimating the transition temperature using loop-TNR. We set $T^- = 2.66$ and $T^+ = 2.68$ as an initial estimate. The level-crossing temperature $T^*(L)$ is linearly fitted to extrapolate the transition temperature. The insert shows how we compute $T^*(L)$ for various system sizes.

they have scaling dimension 4, the corresponding coupling constant is renormalized as $g \propto L^{-2}$. This leads to an error of $O(L^{-2})$ in the naive estimate of the critical point using $\delta x_\sigma(L) = 0$.

We can improve the accuracy by removing the effects of the leading irrelevant perturbation g. This can be done by combining the shifts of the rescaled energy levels $\delta x_\sigma(L)$ and $\delta x_\epsilon(L)$ as

$$\delta x_{\text{cmb}} \equiv \delta x_\sigma(L) + \frac{1}{16}\delta x_\epsilon(L)$$
$$= \pi g_\epsilon + \left(\alpha_\sigma^\sigma + \frac{1}{16}\alpha_\epsilon^\sigma\right)g_\sigma^2 + \left(\alpha_\sigma^\epsilon + \frac{1}{16}\alpha_\epsilon^\epsilon\right)g_\epsilon^2. \quad (14)$$

Note that the first-order correction in the irrelevant coupling g is canceled out. Now we can identify the critical point by finding the temperature for which $\delta x_{\text{cmb}} \propto g_\epsilon(L) = 0$. Having eliminated the effects of the leading irrelevant perturbation T_{cyl}^2, $\bar{T}_{\text{cyl}}^2$, the dominant error is now caused by the next-leading irrelevant operator with scaling dimension 6 and thus should be scaled as L^{-4}.

In practice, the determination of the critical point can be efficiently implemented as follows. First, we pick up one temperature from each phase: $T^+ > T_c$ and $T^- < T_c$, and calculate the combined shift δx_{cmb} at these temperatures. The phase of the system can be confirmed by observing the growth of δx_{cmb} as the system size increases because it increases (decreases) if the system is in the high-temperature (low-temperature) phase (if the initial choice of the temperature turns out to be wrong, change the temperature and restart the process). Next, linear interpolations of the combined shift between the two temperatures $T^\pm$ are made, and the crossing of the lines for system sizes L and $\sqrt{2}L$ is found, as shown in the insert of Fig. 2. We denote the temperature where the two
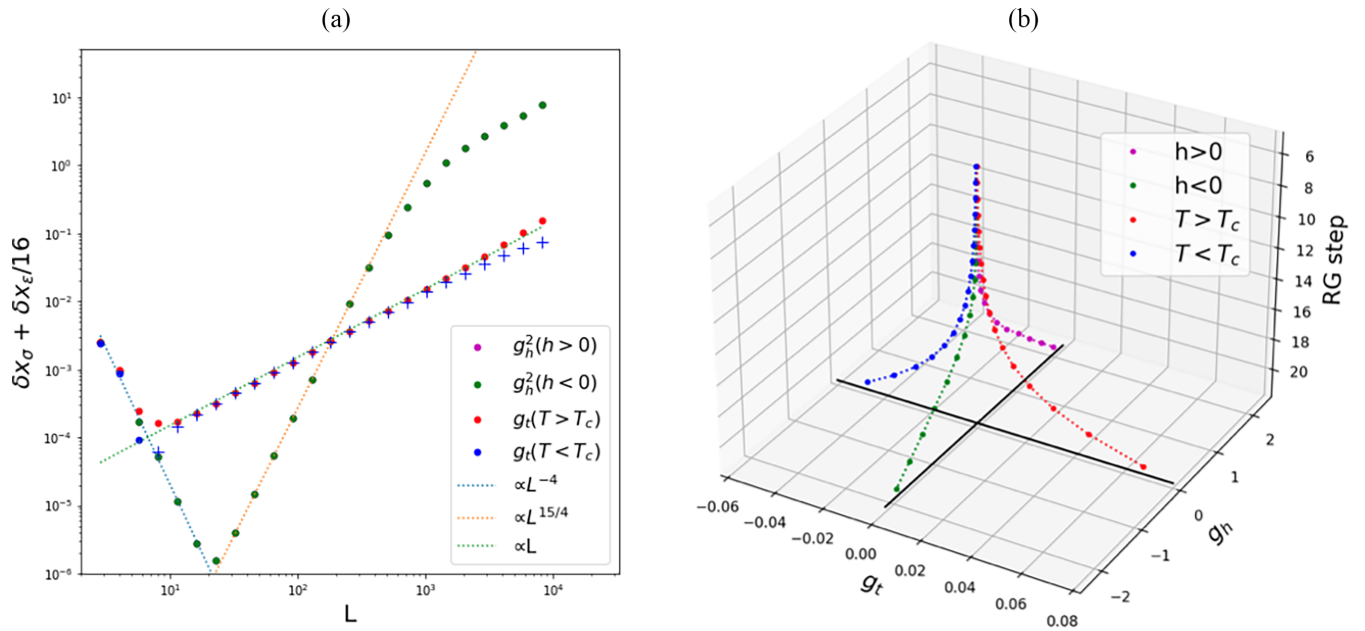
---

[4]As T_{cyl}^2 and $\bar{T}_{\text{cyl}}^2$ are not primary operators, we need to pay special attention. The details are discussed in the Appendix.

(a) (b)

FIG. 3. (Left panel) The system-size dependence of $\delta x_{\mathrm{cmb}} = \delta x_\sigma + \delta x_\epsilon/16$ for $h = \pm 10^{-5}$ (purple and green), $T = 1.0001 T_c$ (red), and $T = 0.9999 T_c$ (blue). The purple and green dots are on top of each other, and "+" denotes the data with a negative sign. After removing the L^{-2} irrelevant perturbations, the next-leading L^{-4} perturbation shown with a blue dotted line appears. The data were obtained via loop-TNR with a bond dimension of $D = 24$, which was deemed sufficient for the finitely correlated systems being considered. (Right panel) The resulting renormalization group flow. Only data after six steps are exhibited, where the L^{-4} perturbations disappear.

lines cross as $T^*(L)$. Because of the second-order contribution $O(g_\epsilon^2)$ in Eq. (14), the crossing temperature $T^*(L)$ obtained by the *linear* interpolation deviates from the true critical point T_c as $T^*(L) - T_c \propto g_\epsilon \propto L$, when $g_\epsilon \ll 1$.[5] The critical point T_c is estimated by fitting $T^*(L)$ by a linear function of L as $T^*(L) \sim T_c + \mathrm{const}\, L$. While the "extrapolation" to $L = 0$ used here might look unusual, this procedure is done to remove the effect of the nonlinearity due to $O(g_\epsilon^2)$ in Eq. (14), and the condition $\delta x_{\mathrm{cmb}} = 0$ itself is accurate for T_c up to the error of $O(L^{-4})$ due to the next-leading irrelevant perturbations. An example of the estimate of T_c with the above procedure with the choice of the temperatures $T^+ = 2.68$ and $T^- = 2.66$ and with system sizes $16 \leqslant L < 64$ is depicted in Fig. 2. The final estimate of the critical point is $T_c^{\mathrm{est}} = 2.269\,177$. Remarkably, even with the choice of two temperatures differing by 10^{-2} and the relatively low bond dimension $D = 20$, the estimated critical point is quite accurate: $T_c^{\mathrm{est}} - T_c = -8.11 \times 10^{-6}$. This is thanks to the suppression of the error to $O(L^{-4})$ by eliminating the contributions from the leading irrelevant operators. Once the critical point is estimated with good accuracy with this procedure, the accuracy can be further improved by choosing $T^\pm$ closer to the estimated critical temperature and then applying the same procedure.

D. Renormalization group flow

The comparison between the TNR spectrum (6) and the conformal perturbation theory (8) can also be used to extract

running coupling constants and their scale dependence, enabling a visualization of the RG flow. While this was shown for the BKT transition in the XY model [16], here let us demonstrate the method for the Ising model. This will also be useful to investigate the finite bond dimension effects in detail, as we will discuss in Sec. IV. The extraction of running coupling constants in the Ising model is again based on the shifts of the rescaled energy levels in Table II, and it is useful to consider the combined shift (14) also for this purpose. Given g_σ and g_ϵ are small in the vicinity of criticality, we neglect g_ϵ^2 for $h = 0$ and redefine two relevant coupling constants as

$$g_t = \pi g_\epsilon \quad \text{and} \quad g_h = \sqrt{\left(\alpha_\sigma^\sigma + \frac{1}{16}\alpha_\epsilon^\sigma\right)}\, g_\sigma \text{ for convenience. In this}$$

way, the combined shift (14) simply gives g_t when $h = 0$ and g_h^2 when $T = T_c$, in the lowest order of g_t, g_h. Using these relations, we can read off the relevant coupling constants g_t or g_h from the TNR data, as shown in Fig. 3(b). As we have discussed in the previous subsection, the effects of the leading irrelevant perturbations $T_{\mathrm{cyl}}^2, \bar{T}_{\mathrm{cyl}}^2$ with scaling dimension 4 are eliminated in the combined shift (14), and thus the finite-size correction is now of $O(L^{-4})$, due to the next-leading irrelevant operators with scaling dimension 6. This $O(L^{-4})$ scaling is indeed observed in Fig. 3 near the critical point for small system size L when relevant perturbations are still negligible. Since it is safe to say that these contributions disappear after five RG steps, we can conclude that the origin of g_t and g_h is purely from ϵ and σ after six steps.

The right panel illustrates the scale dependence of the coupling constants g_t and g_h. It is nothing but the RG flow of the Ising critical point, and we conclude that we succeed in calculating the RG flow of the celebrated Ising fixed point.

There is one thing to note on the left panel of Fig. 3. While the combined shift (14), which is an estimator for $|g_h|^2$,

---

[5]It is proportional to $L^{2-x_{\mathrm{thermal}}}$, where x_{thermal} is the scaling dimension of the thermal operator.

scales as $L^{3.75}$ at $L < 10^3$, it starts to flatten and scales as L at $L > 10^3$. This behavior has a rather simple origin. Since the magnetic perturbation is relevant, the system has a finite correlation length or, equivalently, a nonzero gap Δ. This implies that the rescaled energy levels are proportional to L for sufficiently large system size $L \gg \Delta^{-1}$, as mentioned in Sec. III A. As a consequence, the shift (14) also grows proportionally to L. In this regime, the conformal perturbation theory breaks down (higher-order contributions are important), and we no longer identify the shift (14) with $|g_h|^2$. This should be distinguished from the L-linear behavior of the combined shift (14) observed for $L > 10$ with $h = 0$ and $T \neq T_c$, which corresponds to the renormalization of $g_t \propto L$ because of $x_\epsilon = 1$. The L-linear behavior due to the gap is observed in the nonperturbative regime $\delta x_{\epsilon,\sigma} \gg x_{\epsilon,\sigma}$, whereas the L-linear behavior due to the scaling is observed in the perturbative regime $\delta x_{\epsilon,\sigma} \ll x_{\epsilon,\sigma}$.

IV. FINITE BOND DIMENSION EFFECTS

Let us examine the impacts of a finite bond dimension D on TNR from the perspective of our method. In any computation that employs tensor networks, it is necessary to restrict the bond dimension to a finite value D due to the increasing storage requirements and computational costs associated with larger bond dimensions. The finiteness of the bond dimension inevitably leads to a loss of information in each step of renormalization after a certain number of iterations. Although TNR can nominally handle arbitrary large systems, and the TNR-type calculations are often used to study extremely large systems, we have to be careful about the limitations due to the finite bond dimension.

The limitation of the finite bond dimension D on the MPS is characterized by the finite (maximum) correlation length $\xi(D)$ of the MPS [31–33]. The correlation length of MPS is known to obey the scaling law

$$\xi(D) \sim D^\kappa, \tag{15}$$

$$\kappa = \frac{6}{c\left(1 + \sqrt{\frac{12}{c}}\right)}. \tag{16}$$

While the TNR-type calculation of two-dimensional statistical systems appears rather different from the MPS applied to one-dimensional quantum systems, the emergence of the finite correlation length $\xi(D)$ obeying the similar scaling law (15) was reported in Ref. [34] for a HOTRG calculation of the critical Ising model in two dimensions. The exponent κ for the Ising model was estimated to be approximately 2, which is close to the MPS exponent (16) $\kappa = 2.03425\ldots$ for the Ising CFT with central charge $c = \frac{1}{2}$. A similar emergence of the finite correlation length $\xi(D)$ was also reported in our TNR finite-size scaling study of the two-dimensional XY model [16], with the MPS exponent (16) for $c = 1$.

In the following, using our TNR finite-size scaling methodology, we will demonstrate that the emergence of the finite correlation length due to the finite bond dimension in TNR can be attributed to an emergent relevant perturbation (Sec. IV A). Furthermore, we present evidences for the scaling (15) with
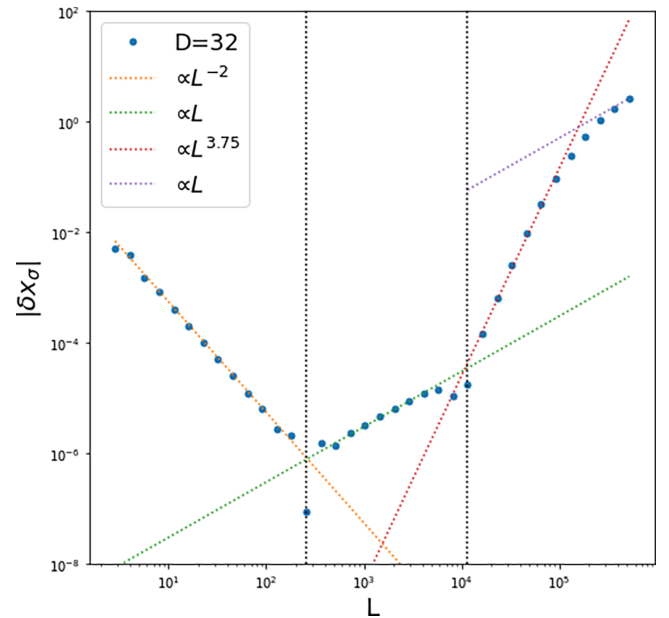

FIG. 4. Shift $|\delta x_\sigma(L)|$ for the Ising model at $T = T_c, h = 0$ computed by loop-TNR with $D = 32$. There is little finite-D effect for small system sizes $L < 256$. The emergent perturbations of ϵ and σ appear at $L \sim 256$ and $L \sim 10^4$, scaling as L and $L^{15/4}$. The induced gap by finite D goes towards constant at $L > 10^5$ as denoted with the purple dotted line.

the MPS exponent (16) in TNR of Ising and three-state Potts models (Sec. IV B).

A. Emergent relevant perturbation

If a finite correlation length emerges in the TNR, it would be natural to identify the renormalized tensor with a Hamiltonian for the system away from the critical point, that is, an RG fixed-point (CFT) Hamiltonian perturbed with relevant operators

$$H_{\text{FB}}(D) = H_{\text{CFT}}^* + \sum_i \int_0^L dx\, g_i(D, L)\Phi_i(x, D), \tag{17}$$

where H_{FB} is the effective Hamiltonian of the finite-D system and $\Phi_i(x, D)$ are the scaling operators representing the perturbations. In this view, we expect relevant perturbations to emerge in order to mimic the finite correlation length imposed by the finite bond dimension.

To demonstrate the emergence of the relevant perturbation, we investigate the system-size dependence of the shift in the rescaled energy levels δx_σ. In Fig. 4, we show the absolute value of the shift $|\delta x_\sigma|$ as a function of the system size L used in calculating the transfer matrix spectrum in TNR exactly at the critical point $h = 0, T = T_c$. The conformal perturbation theory in Eq. (8) implies that the shift x_σ contains contributions from the irrelevant perturbations. Since the leading irrelevant operators at the critical points are T_{cyl}^2 and $\bar{T}_{\text{cyl}}^2$ with scaling dimension 4, we expect $\delta x_\sigma(L)$ decays as L^{-2}. [This is to be contrasted with Eq. (14) and Fig. 3, in which the contributions from T_{cyl}^2 and $\bar{T}_{\text{cyl}}^2$ are eliminated.] The expected L^{-2} behavior in the shift $\delta x_\sigma(L)$ is indeed observed for small
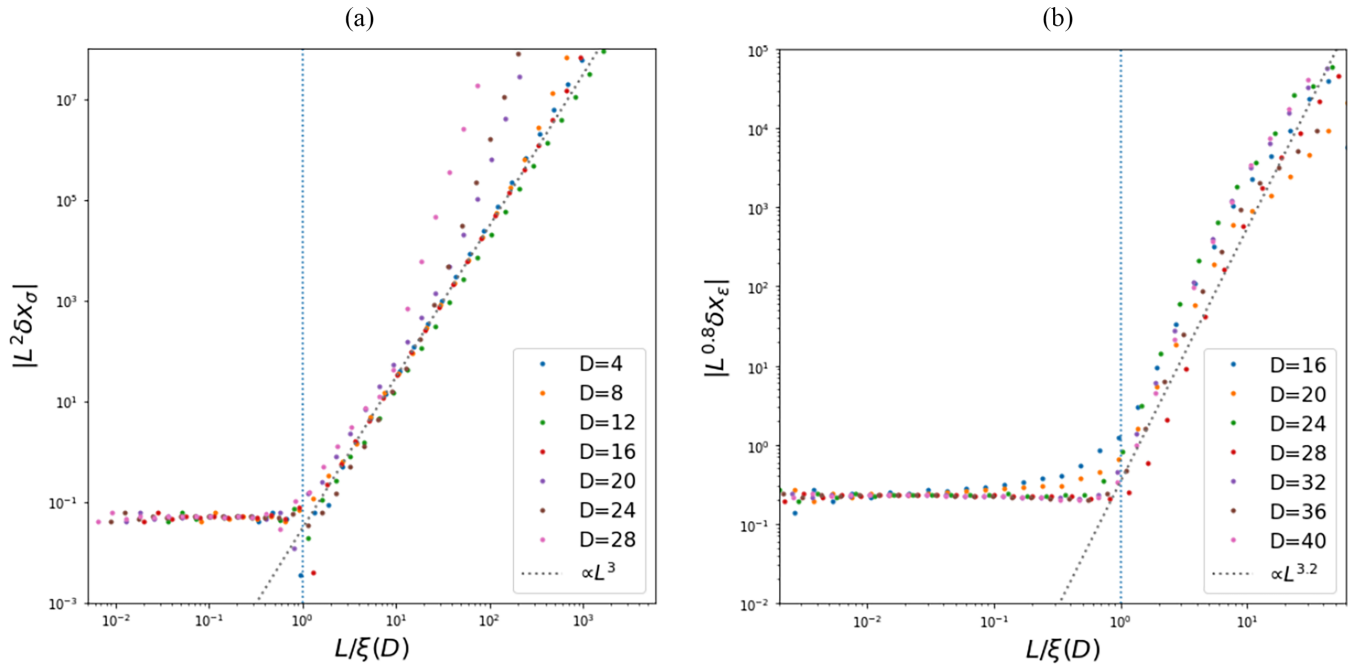
(a)

(b)

FIG. 5. (a) The scaling of the shift δx_σ in TNR of the Ising model at the critical point, for various bond dimensions $D = 4, \ldots, 28$. The vertical axis is scaled as $L^2 \delta x_\sigma$ so that it is constant when $L \ll \xi(D)$. When $L \ll \xi(D)$, the shift is dominated by the emergent relevant perturbation ϵ; this is confirmed by the scaling $L^2 g_\epsilon \propto L^3$. The horizontal axis is scaled as $L/\xi(D)$, where the correlation length $\xi(D)$ is hypothesized as in Eqs. (15) and (16). The collapse of the data for different bond dimensions is strong evidence of the hypothesized scaling of the correlation length $\xi(D)$. The blue dotted line indicates $L/\xi(D) = 1$. We set $\xi(D) = 2.0 D^\kappa$ so that $L/\xi(D) = 1$ becomes the crossover scale between the finite-size scaling regime and the finite-D scaling regime. (b) Similar scaling analysis of the shift δx_ϵ in TNR of the three-state Potts model at the critical point, for various bond dimensions $D = 16, \ldots, 40$ with $\xi(D) = 0.067 D^\kappa$. The scaled shift $L^{0.8} \delta x_\epsilon$ behaves as a constant in the finite-size scaling regime $L/\xi(D) < 1$, whereas it scales as $L^{3.2}$ in the finite-D scaling regime $L/\xi(D) > 1$, as expected from the CFT analysis (see Appendix for details). The data for different bond dimensions collapse again, giving compelling evidence for the scaling of the correlation length (15) and (16).

system sizes $L < 256$. For larger system sizes, however, $|\delta x_\sigma(L)|$ starts to increase, deviating from the conformal perturbation theory scaling L^{-2}. We identify the finite bond dimension D effects as the origin of this deviation. More remarkably, we can observe a clear scaling behavior of the deviation. That is, the shift $|\delta x_\sigma(L)|$ scales with the system sizes as L and $L^{15/4}$ for $256 < L < 10^4$ and $10^4 < L$, respectively. Compared with the off-critical cases in Fig. 3, we realize that these scalings are identical to those induced by the thermal and magnetic perturbations. In other words, the relevant perturbations emerge in the TNR calculation.

Let us first discuss the $L^{15/4}$ scaling of the shift, observed for $L > 10^4$. This can be understood as the effect of an emerging magnetic perturbation h. Although the magnetic perturbation h is forbidden by the $\mathbb{Z}_2$ spin-flip symmetry, the symmetry could be broken by the limitations in the machine precision. Once the spin-flip symmetry is broken, the magnetic field h, which is a relevant perturbation, is effectively generated. Even if the effective magnetic field h is extremely small, it will be enhanced at each RG step and eventually dominates the system at sufficiently large length scales. This is what we observe for $L > 10^4$. This phenomenon should be related to machine precision and not intrinsic to the algorithm. If we are interested in a $\mathbb{Z}_2$ symmetric system, we can impose the symmetry at each step of TNR in order to avoid this effect.

In contrast, the L scaling observed for $256 < L < 10^4$ is more intrinsic. The most relevant perturbation allowed under

the $\mathbb{Z}_2$ symmetry to the critical Ising fixed point is the thermal operator. Thus, we expect that the finite bond dimension effect can be mimicked by the thermal perturbation ϵ to the fixed-point Hamiltonian H^*_{CFT}. If this is the case, the effective coefficient g_ϵ grows proportionally to L as the system size L is increased because the thermal operator ϵ has the scaling dimension 1. According to Eq. (8), this will lead to a correction proportional to L in the rescaled energy level $\delta x_\sigma(L)$. This is indeed supported by the numerical result shown in Fig. 4.

In general, the finite-D effect in TNR would be described in terms of the emergence of relevant perturbation(s) to the fixed-point Hamiltonian, which induces the finite correlation length $\xi(D)$. In addition to the emergence of the relevant operator ϵ in the critical Ising model discussed above, a similar emergence of the relevant operator is observed in the critical three-state Potts model, as demonstrated in the Appendix.

B. Scaling of the emergent correlation length

Now let us demonstrate that the finite correlation length $\xi(D)$ induced by the finite bond dimension D in TNR obeys the same scaling (15) and (16) as in the MPS, as suggested in Refs. [16,34].

In Fig. 5, we demonstrate the scaling of the correlation length induced by the finite bond dimension in TNR of the critical Ising and the three-state Potts models. In Fig. 5(a), we plot the shift δx_σ in the Ising model obtained by the TNR of

the Ising model at the critical point, which was also studied in Fig. 4, with several different bond dimensions $D = 4, \ldots, 28$. Here, we rescaled the vertical axis as $L^2 \delta x_\sigma$ so that the constant behavior is observed for system size smaller than the correlation length, where the leading irrelevant perturbation (which causes $\delta x_\sigma \propto L^{-2}$) is dominant. The deviation from the constant at larger system sizes L can be attributed to the emergent relevant perturbation ϵ induced by the finite bond dimension D, as discussed in the previous subsection. This is confirmed by the L^3 scaling (L^2 times $\delta x_\sigma \propto g_\epsilon \propto L$). Most importantly, the horizontal axis is the rescaled system size $L/\xi(D)$ using the hypothesized correlation length $\xi(D) = aD^\kappa$ given by Eqs. (15) and (16). The collapse of the data for different bond dimensions strongly supports our hypothesis on the correlation length. Note that we roughly fit the prefactor a so that the crossover occurs at $L = \xi(D)$.

In order to confirm the finite-D scaling of the correlation length and its universality, we have also studied the three-state Potts model at the critical point. As an example, in Fig. 5(b), we plot the shift of the rescaled energy level corresponding to the energy operator ϵ in the three-state Potts model. For this shift δx_ϵ, the contribution from the leading irrelevant operator is $\sim L^{-4/5}$, and the dominant contribution from the emergent relevant perturbation ϵ is expected to be proportional to $g_\epsilon{}^2 \propto L^{12/5}$. (See the Appendix for details.) We rescaled the vertical axis as $L^{0.8} \delta_\epsilon$ so that it is constant in the finite-size scaling regime $L < \xi(D)$. The horizontal axis is again the rescaled system size $L/\xi(D)$, with the correlation length $\xi(D)$ defined in Eqs. (15) and (16) with the central charge $c = \frac{4}{5}$ for the three-state Potts model. The data for different bond dimensions again show a collapse, providing compelling evidence for our hypothesis on the correlation length scaling. For $L/\xi(D) > 1$, the data fit well the expected behavior $L^{0.8} \times g_\epsilon{}^2 \propto L^{0.8} \times L^{2.4} = L^{3.2}$.

V. CONCLUSION AND DISCUSSION

In the first part of the paper, we discussed a method for computing the coupling constants using renormalized tensors based on the finite-size scaling theory of CFT. By plotting the resulting values at each scale, we were able to visualize the RG flow, and we confirmed that the theoretical RG flows, as shown in Fig. 3, are consistent with the Ising and XY models. Our method has the advantage of being able to extract both ultraviolet and infrared information, making it a valuable tool for investigating gapped and crossover systems.

In the second part of the paper, applying the methodology developed in the first part, we explored the impact of finite bond dimension D on the RG flow. The finiteness of the bond dimension results in a finite correlation length $\xi(D)$ or, equivalently, in a nonzero gap in the energy spectrum of the corresponding one-dimensional quantum system. We find that this gap formation can be attributed to the emergence of a relevant perturbation enforced by the finite bond dimension. This is demonstrated by the RG flow of the emergent relevant coupling.

The finite-size scaling of TNR shows a crossover at $L \sim \xi(D)$, above which the system is governed by the finite correlation length. The correlation length $\xi(D)$ induced by the finite bond dimension in TNR shows the same scaling (15),
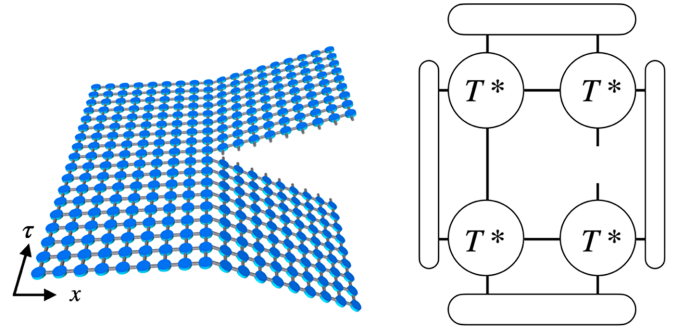

FIG. 6. (Left panel) A schematic picture of the reduced density matrix ρ_A for a bipartition of the system in the path-integral picture. The uncontracted legs correspond to the indices of the reduced density matrix. (Right panel) Each of the four quadrants of the space-time in the left panel may be replaced by the renormalized tensor in TNR with appropriate boundary conditions.

(16) as the correlation length of MPS. While such scaling in TNR was suggested earlier in Refs. [16,34], in this paper, we presented more convincing evidence.

Although we do not have a mathematical proof for the scaling of $\xi(D)$ in TNR at this point, it may be natural from the following point of view. Aside from the construction of the transfer matrix by contracting horizontal legs, the renormalized tensor obtained in TNR can give the corner transfer matrix by contracting the upper and left legs. The same finite-D scaling (15), (16) as in MPS was observed in corner transfer matrix renormalization group (CTMRG) [35–37]. Moreover, the entanglement spectrum for the half-bipartition of the system of length $2L$ can be related to a contraction of four renormalized tensors of linear size L [38], as shown in Fig. 6. These relations are suggestive of the identical scaling of $\xi(D)$ in MPS, CTMRG, and TNR as we have observed.

Our study highlights the importance of considering the impact of the finite bond dimension in the TNR-type approach. In particular, a direct study of the thermodynamic limit with TNR would be prone to errors due to the finite correlation length $\xi(D)$ imposed by the finite bond dimension. As a resolution of this problem, we have demonstrated that accurate data for the thermodynamic limit can be extracted by finite-size scaling of TNR spectra obtained for system sizes smaller than $\xi(D)$, combined with conformal field theory. Even with this limitation, the tractable system size is greatly increased from $\sim \log D$ with exact diagonalization to $\xi(D) \sim D^\kappa$ in TNR.

Note added. Recently, a closely related work [39] based on a HOTRG study of the Ising model appeared. It is quite similar in spirit to this work, combining finite-size scaling and HOTRG. Their estimate of the correlation length ξ from the transfer matrix eigenvalue, and the determination of the critical point based on the finite-size scaling of ξ, are essentially equivalent to our analysis of δx_σ discussed in Sec. III C. Utilizing the knowledge of Ising CFT, we have further improved the accuracy by analyzing δx_{cmb} which removes the effects of the leading irrelevant operators. The error in the estimated transition temperature T_c^{est} we obtained in Sec. III C is about 10^{-5}, which is larger than theirs ($10^{-7} \sim 10^{-6}$). However, our estimate is based on the data at two temperatures

$T^{\pm}$ separated by 10^{-2} and can be further improved by taking more data points. The MPS scaling (15) and (16) of the correlation length in TNR we have discussed is also supported by them.

APPENDIX: FINITE-ENTANGLEMENT SCALING OF THE THREE-STATE POTTS MODEL

1. Model

We can further verify the emergence of relevant perturbations by applying it to the three-state Potts model. It is a natural extension of the Ising model to the $\mathbb{Z}_3$ symmetry, and the Hamiltonian is

$$H = -\sum_{\langle i,j \rangle} \delta_{s_i,s_j}, \tag{A1}$$

where s_i takes 0, 1, and -1. It has a phase transition of $\mathbb{Z}_3$ symmetry breaking at $T_c = 1/\log(1 + \sqrt{3})$. The critical theory of the three-state Potts model is another type of the minimal model $\mathcal{M}(6, 5)$ with $c = \frac{4}{5}$ [18,40]. A set of primary operators are shown in Table III.

As opposed to the Ising model, there are off-diagonal operators as $\Phi_{\frac{2}{5},\frac{7}{5}}$, $\Phi_{\frac{7}{5},\frac{2}{5}}$, and $\Phi_{3,0}$, $\Phi_{0,3}$ (currents). Let us first examine the RG flow in a gapped system. Similar to the Ising model, the phase transition is identified by spontaneous symmetry breaking. The high-temperature phase is a trivial phase, whereas the low-temperature region is $\mathbb{Z}_3$ symmetry-breaking phase. Thus, the fixed-point tensor is a stacking of three states with their $\mathbb{Z}_3$ charge 0, -1, and 1.

2. Construction of the effective Hamiltonian

The RG flow can be seen by investigating the scaling dimensions. For instance, we can take the spin operator $\sigma =$

TABLE III. A set of primary operators of the three-state Potts model.

Symbol	Dimension	Meaning
I	0	Identity
ϵ	$\frac{2}{5}$	Thermal op.
σ	$\frac{1}{15}$	Spin
X	$\frac{7}{5}$	
Y	3	
Z	$\frac{2}{3}$	

$\Phi_{\frac{1}{15},\frac{1}{15}}$ and plot the value of $\delta x_\sigma = x_\sigma(L) - \frac{2}{15}$. Similarly, as in the Ising model, there is competition between irrelevant and relevant operators: $X = \Phi_{\frac{7}{5},\frac{7}{5}}$ and $\epsilon = \Phi_{\frac{2}{5},\frac{2}{5}}$. The thermal operator separates the $\mathbb{Z}_3$ symmetry-breaking phase from the trivial one. The finite-size corrections of X and ϵ to x_σ are $L^{-0.8}$ and $L^{1.2}$, respectively. The fusion rules are $\sigma \times \sigma = 1 + \epsilon + \sigma + X + Y + Z$, $\epsilon \times \epsilon = 1 + X$, and $\epsilon \times \sigma = \sigma + Z$. Hence, δx_σ has the following form:

$$\delta x_\sigma = 2\pi c_{\sigma\sigma X} g_X \left(\frac{L}{2\pi}\right)^{-0.8} + 2\pi c_{\sigma\sigma\epsilon} g_\epsilon \left(\frac{L}{2\pi}\right)^{1.2}. \tag{A2}$$

On the other hand, the perturbation of ϵ appears as a second-order term for δx_ϵ because the fusion rule says $\epsilon \times \epsilon = 1 + X$. Consequently, δx_ϵ can be computed as

$$\delta x_\epsilon = 2\pi c_{\epsilon\epsilon X} g_X \left(\frac{L}{2\pi}\right)^{-0.8} + \alpha g_\epsilon^2 \left(\frac{L}{2\pi}\right)^{2.4}, \tag{A3}$$

where α is a constant determined from the second-order calculation.

Figure 7 shows the computed δx_σ by TNR. As expected, it exhibits the competition between irrelevant and relevant operators. The sign of g_ϵ is the opposite between two phases, which is a manifest indication of the RG flow in the opposite direction due to the thermal operator. x_σ has doubly degenerate states with $\mathbb{Z}_3$ charge ± 1. In the low-temperature phase, these two states flow to $x_\sigma(L) \to 0$, and the fixed-point tensor becomes threefold degenerate. As for the irrelevant perturbation, there seems to be a discrepancy between δx_σ in Fig. 7 and Eq. (A2). The data points are scattered for small system sizes and not precisely on the fitting lines. This is due to the leading irrelevant operator we have not considered. We can identify it as $T_{\text{cyl}}^2 + \bar{T}_{\text{cyl}}^2$ as following. Just as we did in the left panel of Fig. 3, the contributions from g_X can be eliminated by combining δx_σ and δx_ϵ. The OPE coefficients for the three-state Potts model are known, and the ratio of the two OPE coefficients is $c_{\epsilon\epsilon X}/c_{\sigma\sigma X} = 36$ [41–45]. Thus, the origin of the "scattering" shall be observed by plotting $36\delta x_\sigma - \delta x_\epsilon$.

Figure 8 displays the result for the high-temperature phase. It is now obvious that the scattering of Fig. 7 comes from the L^{-2} perturbation denoted with the red dotted line. Also, it has a conformal spin s because it flips a sign at each step and $s \equiv 4$ (mod 8).[6] As a result, we can conclude the irrelevant operator has the conformal weights as $(h, \bar{h}) = (4, 0)$ and $(0,4)$, which are T_{cyl}^2 and $\bar{T}_{\text{cyl}}^2$. Finally, the effective Hamiltonian of the critical three-state Potts model on the square lattice can be constructed as

$$H = H_{\text{Potts}}^* + \int_0^L dx \left[g_X \Phi_{\frac{7}{5},\frac{7}{5}}(x) + g_T \left(T_{\text{cyl}}^2 + \bar{T}_{\text{cyl}}^2\right) \right]. \tag{A4}$$

---

[6]For each iteration, the lattice rotates by $45°$, and it corresponds to the conformal transformation $w = e^{\frac{i\pi}{4}} z$ on a complex plane. As the irrelevant perturbations T_{cyl}^2 and $\bar{T}_{\text{cyl}}^2$ have a conformal spin 4 and -4, they get an additional factor $(e^{\frac{i\pi}{4}})^4 = (e^{\frac{i\pi}{4}})^{-4} = -1$ for an odd number of steps. We can see this by plotting the data from even steps (original) and odd steps (tilt) separately.
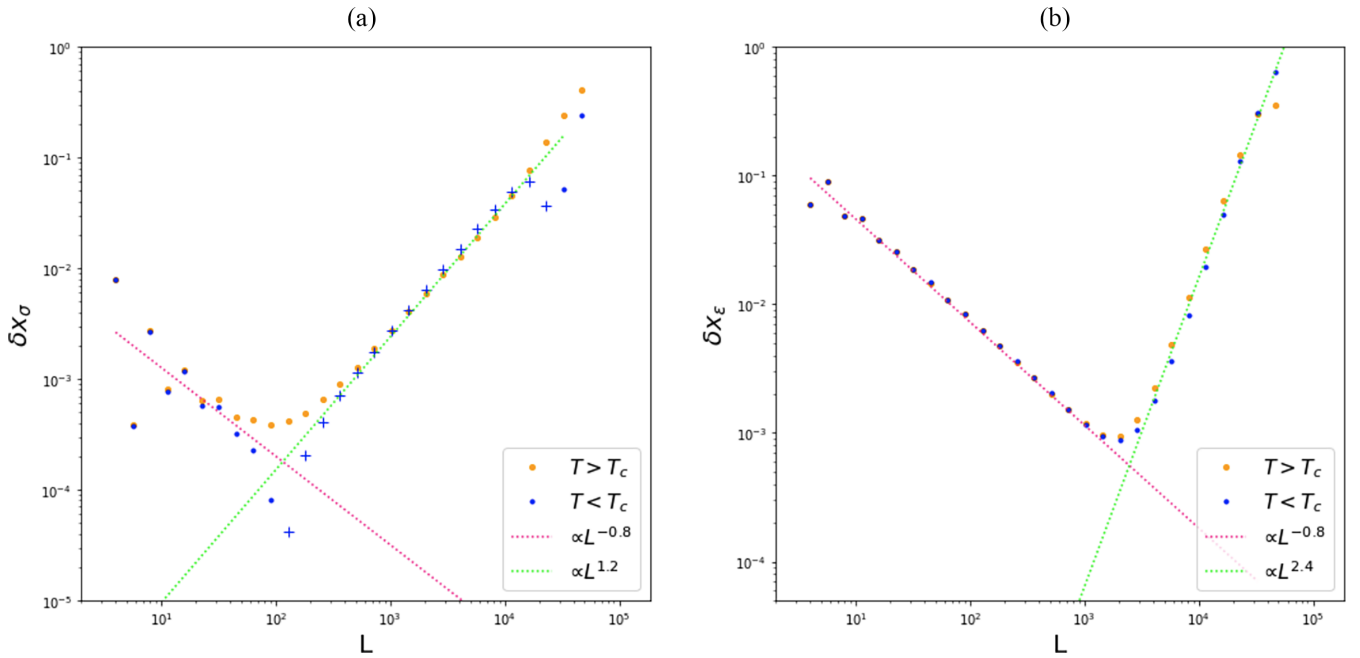
(a)

(b)

FIG. 7. The size dependence of the (a)δx_σ and (b)δx_ϵ at $T = 0.999995T_c$ and $T = 1.000005T_c$. The pink and green dotted lines denote $L^{-0.8}$, (a)$L^{1.2}$, and (b)$L^{2.4}$ fittings respectively. For the low-temperature phase, the sign of δx_σ is negative at $L > 100$. The dip on the left panel around $L \sim 10^2$ corresponds to the zero point of Eq. (A2). (b) The finite-size effect to the x_ϵ suffers less from $T_{\text{cyl}}^2 + \bar{T}_{\text{cyl}}^2$ in amplitude. The scaling of Eq. (A3) is clearly observed.

3. Finite-entanglement scaling

At the critical temperature of the Ising model, the finite-D effect proves to be a perturbation from the thermal operator. Let us verify it for the critical three-state Potts model. Due to the irrelevant perturbations from $T_{\text{cyl}}^2 + \bar{T}_{\text{cyl}}^2$, the finite-$D$

effects are clearer for $x_\epsilon(L)$ as seen in Fig. 7(b). This is shown in Fig. 5 of the main text. Here, we demonstrate that $\delta x_\sigma(L)$ also shows the universal behavior with $L/\xi(D)$. Figure 9 shows the rescaled correction to $\delta x_\sigma(L)$. For $L > \xi(D)$, the
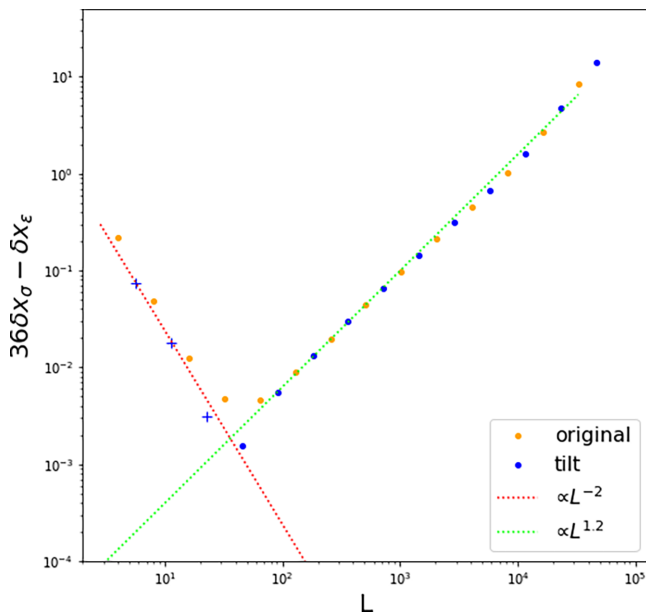

FIG. 8. $36\delta x_\sigma - \delta x_\epsilon$ for the high temperature phase. "+" is used when the sign is negative. The red dotted line denotes the L^{-2} fitting while the light green one is just a relevant $L^{1.2}$ contribution from ϵ. Loop-TNR rotates the lattice by $\frac{\pi}{4}$ at each RG step, and the tilted system is plotted with the blue dots.
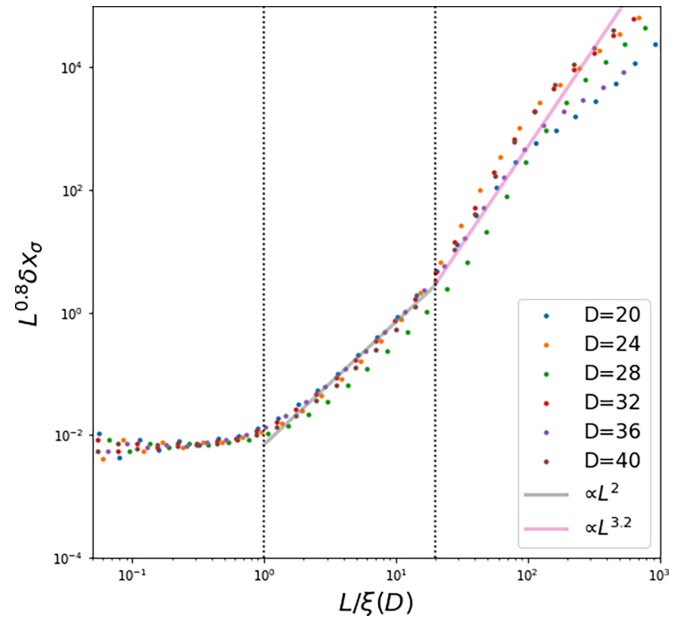

FIG. 9. Rescaled δx_σ by $\xi(D) = D^\kappa$ at the critical temperature. The resulting data collapse onto a universal function that is independent of $L/\xi(D)$. If $L/\xi(D) < 1$, the system is in the FSS region, while if $L/\xi(D) \geqslant 1$, it is in the FES region. In the FES region, the scaling of the first-order and second-order perturbations are indicated by a gray and pink line, respectively. x_σ is computed as an average value of the first and second excitation energy.

perturbation grows as L^2 denoted by a gray line, which means that the emergent perturbation scales as $L^{1.2}$. Compared with Eq. (A2), it is clear that the emergent perturbation is from the thermal operator. However, as the system size increases, the second-order perturbation becomes predominant as shown with a pink line. As ϵ is the most relevant operator that is permitted by symmetry, it supports our conjecture stated in the main text.

[1] K. G. Wilson, Renormalization group and critical phenomena. I. renormalization group and the Kadanoff scaling picture, Phys. Rev. B **4**, 3174 (1971).

[2] K. G. Wilson, Renormalization group and critical phenomena. II. phase-space cell analysis of critical behavior, Phys. Rev. B **4**, 3184 (1971).

[3] K. G. Wilson, The renormalization group: Critical phenomena and the Kondo problem, Rev. Mod. Phys. **47**, 773 (1975).

[4] M. E. Fisher, The renormalization group in the theory of critical behavior, Rev. Mod. Phys. **46**, 597 (1974).

[5] K. G. Wilson and M. E. Fisher, Critical Exponents in 3.99 Dimensions, Phys. Rev. Lett. **28**, 240 (1972).

[6] S. R. White, Density matrix formulation for quantum renormalization groups, Phys. Rev. Lett. **69**, 2863 (1992).

[7] M. Levin and C. P. Nave, Tensor Renormalization Group Approach to Two-Dimensional Classical Lattice Models, Phys. Rev. Lett. **99**, 120601 (2007).

[8] G. Evenbly and G. Vidal, Tensor Network Renormalization, Phys. Rev. Lett. **115**, 180405 (2015).

[9] G. Evenbly, Algorithms for tensor network renormalization, Phys. Rev. B **95**, 045117 (2017).

[10] S. Yang, Z.-C. Gu, and X.-G. Wen, Loop Optimization for Tensor Network Renormalization, Phys. Rev. Lett. **118**, 110504 (2017).

[11] M. Bal, M. Mariën, J. Haegeman, and F. Verstraete, Renormalization Group Flows of Hamiltonians Using Tensor Networks, Phys. Rev. Lett. **118**, 250602 (2017).

[12] M. Hauru, C. Delcamp, and S. Mizera, Renormalization of tensor networks using graph-independent local truncations, Phys. Rev. B **97**, 045111 (2018).

[13] Y. Zou, A. Milsted, and G. Vidal, Conformal Data and Renormalization Group Flow in Critical Quantum Spin Chains Using Periodic Uniform Matrix Product States, Phys. Rev. Lett. **121**, 230402 (2018).

[14] C. Delcamp and A. Tilloy, Computing the renormalization group flow of two-dimensional ϕ^4 theory with tensor networks, Phys. Rev. Res. **2**, 033278 (2020).

[15] K. Nomura and K. Okamoto, Critical properties of s= 1/2 antiferromagnetic XXZ chain with next-nearest-neighbour interactions, J. Phys. A: Math. Gen. **27**, 5773 (1994).

[16] A. Ueda and M. Oshikawa, Resolving the Berezinskii-Kosterlitz-Thouless transition in the two-dimensional XY model with tensor-network-based level spectroscopy, Phys. Rev. B **104**, 165132 (2021).

[17] See https://github.com/dartsushi/Loop-TNR_RGflow.

[18] P. Francesco, P. Mathieu, and D. Sénéchal, *Conformal Field Theory* (Springer, New York, 2012).

[19] J. L. Cardy, Conformal invariance and universality in finite-size scaling, J. Phys. A: Math. Gen. **17**, L385 (1984).

[20] J. L. Cardy, Operator content of two-dimensional conformally invariant theories, Nucl. Phys. B **270**, 186 (1986).

[21] Z.-C. Gu and X.-G. Wen, Tensor-entanglement-filtering renormalization approach and symmetry-protected topological order, Phys. Rev. B **80**, 155131 (2009).

[22] L. P. Kadanoff, Operator Algebra and the Determination of Critical Indices, Phys. Rev. Lett. **23**, 1430 (1969).

[23] K. G. Wilson, Non-lagrangian models of current algebra, Phys. Rev. **179**, 1499 (1969).

[24] G. Evenbly and G. Vidal, Local Scale Transformations on the Lattice with Tensor Network Renormalization, Phys. Rev. Lett. **116**, 040401 (2016).

[25] G. Li, K. H. Pai, and Z.-C. Gu, Tensor-network renormalization approach to the q-state clock model, Phys. Rev. Res. **4**, 023159 (2022).

[26] Z. Y. Xie, J. Chen, M. P. Qin, J. W. Zhu, L. P. Yang, and T. Xiang, Coarse-graining renormalization by higher-order singular value decomposition, Phys. Rev. B **86**, 045139 (2012).

[27] Y. Zou and G. Vidal, Multiboundary generalization of thermofield double states and their realization in critical quantum spin chains, Phys. Rev. B **105**, 125125 (2022).

[28] Y. Zou, Universal information of critical quantum spin chains from wavefunction overlap, Phys. Rev. B **105**, 165420 (2022).

[29] Y. Liu, Y. Zou, and S. Ryu, Operator fusion from wavefunction overlaps: Universal finite-size corrections and application to haagerup model, Phys. Rev. B **107**, 155124 (2023).

[30] A. Poghosyan, Shaping lattice through irrelevant perturbation: Ising model, J. High Energy Phys. 11 (2019) 083.

[31] L. Tagliacozzo, T. R. de Oliveira, S. Iblisdir, and J. I. Latorre, Scaling of entanglement support for matrix product states, Phys. Rev. B **78**, 024410 (2008).

[32] F. Pollmann, S. Mukerjee, A. M. Turner, and J. E. Moore, Theory of Finite-Entanglement Scaling at One-Dimensional Quantum Critical Points, Phys. Rev. Lett. **102**, 255701 (2009).

[33] B. Pirvu, G. Vidal, F. Verstraete, and L. Tagliacozzo, Matrix product states for critical spin chains: Finite-size versus finite-entanglement scaling, Phys. Rev. B **86**, 075117 (2012).

[34] H. Ueda, K. Okunishi, and T. Nishino, Doubling of entanglement spectrum in tensor renormalization group, Phys. Rev. B **89**, 075116 (2014).

[35] T. Nishino, K. Okunishi, and M. Kikuchi, Numerical renormalization group at criticality, Phys. Lett. A **213**, 69 (1996).

[36] H. Ueda, K. Okunishi, R. Krčmár, A. Gendiar, S. Yunoki, and T. Nishino, Critical behavior of the two-dimensional icosahedron model, Phys. Rev. E **96**, 062112 (2017).

[37] H. Ueda, K. Okunishi, K. Harada, R. Krčmár, A. Gendiar, S. Yunoki, and T. Nishino, Finite-m scaling analysis of Berezinskii-Kosterlitz-Thouless phase transitions and entanglement spectrum for the six-state clock model, Phys. Rev. E **101**, 062111 (2020).

[38] P. Calabrese and A. Lefevre, Entanglement spectrum in one-dimensional systems, Phys. Rev. A **78**, 032329 (2008).

[39] C.-Y. Huang, S.-H. Chan, Y.-J. Kao, and P. Chen, Tensor network based finite-size scaling for two-dimensional ising model, Phys. Rev. B **107**, 205123 (2023).

[40] V. Dotsenko, Critical behaviour and associated conformal algebra of the Z_3 potts model, Nucl. Phys. B **235**, 54 (1984).

[41] V. Dotsenko and V. Fateev, Conformal algebra and multipoint correlation functions in 2D statistical models, Nucl. Phys. B **240**, 312 (1984).

[42] V. Dotsenko and V. Fateev, Four-point correlation functions and the operator algebra in 2d conformal invariant theories with central charge $c \leqslant 1$, Nucl. Phys. B **251**, 691 (1985).

[43] V. Dotsenko and V. Fateev, Operator algebra of two-dimensional conformal theories with central charge $c \leqslant 1$, Phys. Lett. B **154**, 291 (1985).

[44] J. Fuchs and A. Klemm, The computation of the operator algebra in non-diagonal conformal field theories, Ann. Phys. **194**, 303 (1989).

[45] I. Esterlis, A. L. Fitzpatrick, and D. M. Ramirez, Closure of the operator product expansion in the non-unitary bootstrap, J. High Energy Phys. 11 (2016) 030.